Macromolecules

pubs.acs.org/Macromolecules Article

Tailoring Polymer Polarity to Regulate Disulfide Accessibility in Redox-Active Particles for Organic Batteries

Hongyi Zhang, Garrett L. Grocke, George Rose, Stuart J. Rowan,* and Shrayesh N. Patel*

Cite This: *Macromolecules* 2024, 57, 10410−10417 Read Online

ACCESS | Metrics & More | Article Recommendations | Supporting Information

ABSTRACT: This study seeks to explore the relationship between particle polarity and the electrochemical accessibility of organodisulfide-based redox-active particles. Micron-sized poly(glycidyl methacrylate) (PMGA) particles were synthesized and subsequently cross-linked with thiadiazole disulfide to produce redox-active particles (DS-RAPs). The residual glycidyl units underwent reactions with various side chains to modulate the polarity of the DS-RAPs. These side chains vary from nonpolar aliphatic *N*-methylbutylamine (MBA) to the more polar oligoethylene glycol amine (EGA) and glycidyl carbonate (GC) moieties. Cyclic voltammetry reveals that functionalization with polar side chains enhances electrochemical accessibility, with DS-RAP$_{GC}$ demonstrating the highest accessibility in both acetonitrile and tetraglyme-based electrolytes. Testing the DS-RAP derivatives as cathode electrodes in a lithium cell with a LiTFSI/tetraglyme electrolyte indicates that DS-RAP$_{GC}$ yields the highest specific capacities, energy efficiency, and best kinetics at 0.1C. Conversely, C-rate dependence measurements show that DS-RAP$_{EGA}$ has higher specific capacities at faster C-rates and is more resilient to mass transport limitations compared to DS-RAP$_{GC}$ and DS-RAP$_{MBA}$. This is attributed to greater electrolyte swelling in DS-RAP$_{EGA}$ and higher ion diffusivity, as evidenced by galvanostatic intermittent titration technique (GITT) measurements. Lastly, long-term cycling tests at 0.1C indicate minimal degradation, with the resulting capacity fade attributed to charge trapping during the continuous reversible oxidation/reduction of disulfides. Overall, these findings contribute significantly to the development of effective RAPs for energy storage applications, highlighting the pivotal role of chemical modifications via side chain engineering in controlling particle polarity to enhance charge transport and overall electrochemical performance.

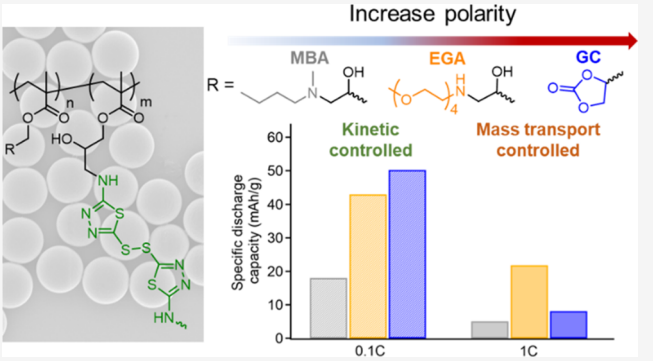

INTRODUCTION

The escalating demand for sustainable and high-performance energy storage systems has pivoted research focus toward the development of innovative materials capable of overcoming the limitations of traditional lithium-ion batteries.[1,2] Organic secondary batteries, utilizing redox-active materials characterized by their metal-free composition, offer a promising pathway toward addressing the dual challenges of environmental sustainability and resource scarcity.[2,3] Among various organic compounds, organosulfur compounds (OSCs), particularly those featuring disulfide bonds, have emerged as a compelling choice for cathode materials.[4−6] Leveraging the reversible two-electron redox behavior of disulfide bonds to store and release energy, OSCs have drawn more attention on account of their high theoretical capacity and average discharge potential, which can lead to higher energy density.

The exploration of organic sulfur compounds (OSCs) as active materials for energy storage technologies has identified several promising candidates for enhancing the performance of lithium batteries. Among the OSCs investigated, tetraethylthiuram disulfide and phenyl disulfide derivatives have been noted for their potential as energy storage molecules. 1,3,4-thiadiazole disulfide (TDDS) and its analogues, notably 2,5-dimercapto-1,3,4-thiadiazole (DMcT), have emerged as standout compounds due to their redox-active properties. These small molecules are particularly compelling for cathode material applications in lithium batteries on account of their capability to reversibly transition between Li−S and disulfide states, which not only facilitates high energy density but also ensures exceptional cyclability. Such properties of DMcT and related compounds underscore their significant potential for advancing lithium battery technologies, promising improvements in both energy storage capacity and longevity.

Despite their promise, the practical application of disulfide bonds in battery technologies is hindered by challenges such as sluggish kinetics and electrode dissolution upon reduction.

Received: August 8, 2024
Revised: October 2, 2024
Accepted: October 7, 2024
Published: October 16, 2024

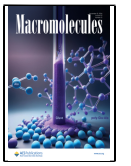

https://doi.org/10.1021/acs.macromol.4c01894
Macromolecules 2024, 57, 10410−10417

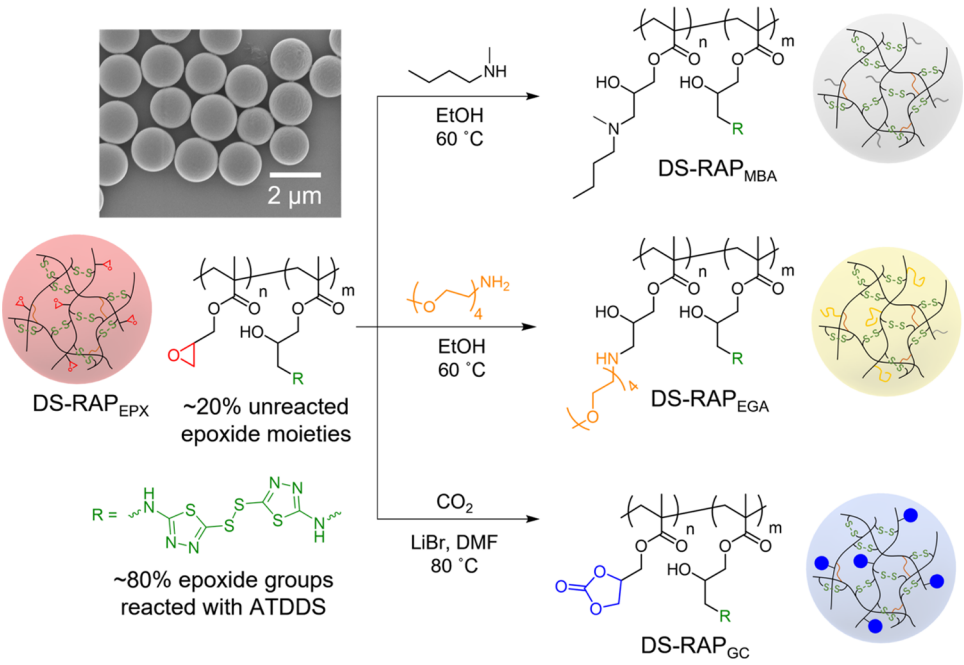

Figure 1. Reaction scheme for the synthesis of DS-RAPs with different side chain moieties. To tune the polarity of the particles, the residual glycidyl epoxy units on DS-RAP$_{EPX}$ were reacted to achieve different side chain functionality. A nonpolar *N*-methylbutylamine (DS-RAP$_{MBA}$) derivative and two polar derivatives: oligoethylene glycol amine (DS-RAP$_{EGA}$) and glycidyl carbonate (DS-RAP$_{GC}$). Top left: SEM image of the DS-RAP$_{EPX}$ before side chain functionalization in the dry state showing a particle diameter of 1.63 ± 0.06 μm.

These challenges lead to limited reversibility and poor conductivity, resulting in diminished battery performance over time. A promising strategy to address these issues lies in incorporating them within polymer architectures.[7−11] For example, by anchoring disulfide moieties as side chains or cross-linkers within polymers, researchers have demonstrated a method to stabilize these active sites, thereby enhancing electrochemical reversibility and mitigating dissolution issues.[12] Despite these advancements, adapting polymer architectures to host redox-active sites introduces a complex array of new challenges. Key among these are the hurdles associated with electrode processing, and electronic and ionic mass transport within the electrode structure that can result in lower-than-theoretical capacities. Redox-active particles (RAPs) have been proposed as a novel solution to these issues, utilizing the structural benefits of polymer networks while improving electrochemical accessibility.[13−18] This strategy aims to optimize the electrochemical performance of organic electrodes by selecting favorable material architectures, paving the way for the realization of high-capacity, efficient energy storage systems.

The poor electronic and ionic conductivities substantially restrict the practical applications of RAPs in battery technologies.[19−21] Numerous studies suggest that optimizing particle size and structure could potentially enhance capacity accessibility, improve cycling stability, and reduce capacity fading.[12,15,17] One possible way to address these challenges is through the engineering of the polymer side chain with multiple attempts made across various chemistries and applications, including mixed ionic−electronic conductors,[22,23] conjugated polymer batteries,[19] and RAPs with proton traps.[24] The focus of the work reported herein aims to evaluate the impact of integrating different side chains, from nonpolar aliphatic moieties to more polar oligoethylene glycol amine (EGA) or glycidyl carbonate moieties (GC), into redox-active polymeric materials. To achieve this, a range of thiadiazole disulfide containing redox-active particles (DS-RAPs) are prepared and characterized using cyclic voltammetry (CV) to evaluate electrochemical behavior and coin cell cycling experiments to evaluate capacity. By examining the effects of side chain modifications on the DS-RAPs' swelling behavior, ion transport, capacity accessibility across various cycling rates, and long-term cycling performance, this investigation not only sheds light on the underlying mechanisms contributing to enhanced capacities but also establishes a foundation for the molecular engineering of organic materials for energy storage.

RESULTS AND DISCUSSION

Synthesis and Characterization of DS-RAPs with Different Side Chain Functionalization. Redox-active bis(5-amino-1,3,4-thiadiazol-2-yl) disulfide (ATDDS) were used to cross-link poly(glycidyl methacrylate) (PGMA) microparticles to yield the (DS-RAPs)[12] (see Supporting Information for more details) with an average dry particle size of 1.63 ± 0.06 μm (Figure 1). Fourier-transform infrared (FT-IR) spectroscopy analysis confirmed the successful functionalization of ATDDS on the PGMA particles, indicated by the reduction in epoxy group signals centered at 846 and 905 cm^{-1}, corresponding to the symmetric and asymmetric stretching of the epoxide groups, respectively (Figures S1 and S2 and Table S1). The synthesized DS-RAP$_{EPX}$ contained approximately 32% ATDDS by mass as determined by UV−vis (eq S1 and Figure S3) with ca. 20% of the epoxide moieties unreacted, which allows for further functionalization of the DS-RAP$_{EPX}$. In this study, three different functionalized DS-RAP$_{EPX}$ were explored, from a nonpolar alkyl chain derived to more polar oligoethylene glycol (DS-RAP$_{EGA}$) and glycidyl carbonate (DS-RAP$_{GC}$) (Figure 1). Reacting the DS-RAP$_{EPX}$ with *N*-methylbutylamine (MBA) yields relatively nonpolar DS-RAP$_{MBA}$, while reaction with 2,5,8,11-tetraoxatridecan-13-

https://doi.org/10.1021/acs.macromol.4c01894
Macromolecules 2024, 57, 10410−10417

amine (EGA) yields the more polar DS-RAP$_{EGA}$. Lastly, glycidyl carbonate functionalized particles DS-RAP$_{GC}$ were synthesized through cycloaddition of CO_2 with the residual epoxides of the DS-RAP$_{EPX}$. The side chain functionalization reactions with MBA, EGA, and CO_2 all proved to be highly efficient, as evidenced by the disappearance of epoxy peaks in the FT-IR spectrum (Figure S1b). The polarity order is assigned as DS-RAP$_{MBA}$ (least polar) < DS-RAP$_{EGA}$ < DS-RAP$_{GC}$ (most polar), based on reported dielectric constants of comparable polymers containing cyclic carbonate and oligo(ethylene glycol).[25,26]

Initial electrochemical characterization was explored through CV using a three-electrode cell setup, with DS-RAPs coated on carbon paper (CP) as the working electrode.[12] The DS-RAPs were first examined in 100 mM tetrabutylammonium hexafluorophosphate ($TBAPF_6$) in acetonitrile (ACN) electrolyte, with a 20 mV/s scan rate (Figure 2a). Experiments are performed using Ag/Ag$^+$ nonaqueous reference electrodes and the potentials are converted to Li/Li$^+$ as the reference potential. All potentials reported in this manuscript are relative to the Li/Li$^+$ reference. DS-RAP$_{EPX}$ exhibited a reduction peak potential ($E_{p,r}$) at 2.92 V, and an oxidation peak potential ($E_{p,o}$) at 3.29 V, with peak-to-peak separation (ΔE_p) of 0.37 V. The DS-RAP$_{MBA}$ CV response resulted in nearly identical redox peak potentials, but with a substantial decrease in measured current density, indicating diminished electrochemical response with the presence of the nonpolar MBA side chain. The more polar DS-RAP$_{EGA}$ CV response showed a slightly shifted $E_{p,r}$ at 2.90 V and $E_{p,o}$ at 3.28 V with a small increase in ΔE_p of 0.38 V. Importantly, it displayed a significant increase in peak current density relative to both DS-RAP$_{EPX}$ and DS-RAP$_{MBA}$, indicating enhanced accessibility to the disulfide redox centers within the particles. The best electrochemical accessibility via CV was seen with DS-RAP$_{GC}$ as demonstrated through the highest measured current density. Moreover, the value of ΔE_p was 0.30 V based on the $E_{p,r}$ at 2.90 V and $E_{p,o}$ at 3.20 V, suggesting comparatively better kinetics with DS-RAP$_{GC}$.

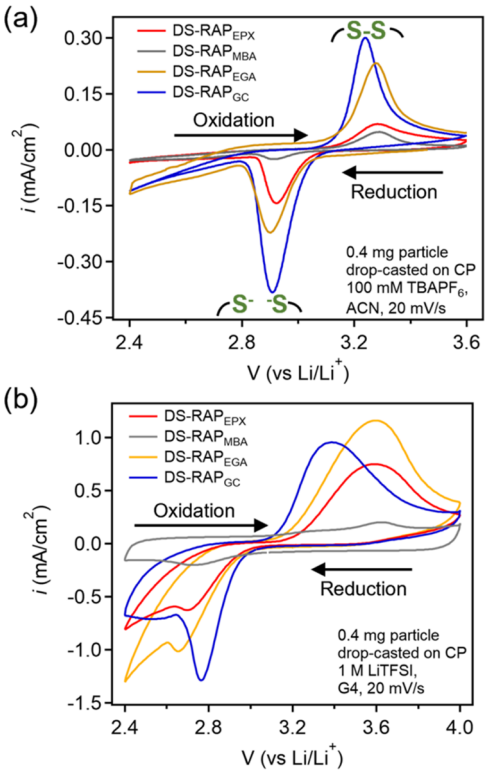

Figure 2. Impact of DS-RAP epoxide functionalization. CV of 0.4 mg of DS-RAP including DS-RAP$_{EPX}$ with residual epoxy groups, nonpolar *N*-methylbutylamine (DS-RAP$_{MBA}$) derivative and two polar derivatives: oligoethylene glycol amine (DS-RAP$_{EGA}$) and glycidyl carbonate (DS-RAP$_{GC}$), cast on carbon paper (CP) in three probe cells in (a) ACN with 100 mM of tetrabutylammonium hexafluorophosphate ($TBAPF_6$) and (b) tetraglyme (G4) with 1 M of lithium bis(trifluoromethane)sulfonimide (LiTFSI). Experiments are performed using Ag/Ag$^+$ nonaqueous reference electrodes, with potentials converted to the Li/Li$^+$ reference, and a scan rate of 20 mV/s.

A similar qualitative trend was observed in the CV response when using 1 M of lithium bis(trifluoromethanesulfonyl)imide (LiTFSI) in tetraglyme (G4), the electrolyte of choice for lithium battery cycling experiments to be discussed later. Overall, DS-RAP$_{GC}$ and DS-RAP$_{EGA}$ demonstrated the best electrochemical performance (Figure 2b). DS-RAP$_{GC}$ exhibited a peak oxidation potential of 3.39 V and a reduction potential of 2.76 V, with peak currents of 0.95 mA/cm^2 for oxidation and −1.29 mA/cm^2 for reduction. Conversely, DS-RAP$_{EGA}$ displayed a peak oxidation potential of 3.60 V with an oxidation peak current of 1.16 mA/cm^2 and a reduction potential of 2.65 V with a peak reduction current of −1.01 mA/cm^2. The differences in reduction current density between DS-RAP$_{EGA}$ and DS-RAP$_{GC}$ stem from their electrolyte conditions. In the LiTFSI electrolyte (Figure 2b), DS-RAP$_{EGA}$ has a higher current density due to better Li$^+$ solvation and higher ion diffusivity, facilitated by the flexible oligoethylene glycol side chains. Conversely, in the $TBAPF_6$/ACN electrolyte (Figure 2a), DS-RAP$_{GC}$ displays a higher current density because its cyclic carbonate side chains interact more effectively in the less coordinating environment, minimizing the impact of ion diffusivity and solvation. This analysis underscores the beneficial impact of incorporating the more polar side chains for optimizing the electrochemical performance of DS-RAPs.

Initial Evaluation of DS-RAPs as Cathodes in Lithium Coin Cells. The electrochemical performance of the different DS-RAPs in a coin cell configuration was explored next, using lithium metal as the anode and the DS-RAPs as the cathode active material (Figure 3a). The cathode preparation involved overnight sonication of DS-RAPs with poly(vinylidene fluoride) (PVDF) binder and carbon black (CB) (at a DS-RAP/CB/PVDF ratio of 90:5:5 wt %) in *N*-methylpyrrolidone (NMP), to yield a homogeneously dispersed mixture. The resultant mixture was then drop-cast onto carbon paper, and dried in a vacuum oven overnight at 55 °C, to form the cathode electrode assembly. The DS-RAP loading was ∼5 mg for all fabricated electrodes. Importantly, the resulting electrode exhibited a uniform morphology with well-distributed DS-RAPs, as illustrated by the SEM image in Figure 3b for DS-RAP$_{GC}$ (corresponding SEMs for DS-RAP$_{MBA}$ and DS-RAP$_{EGA}$ are shown in Figure S4). This uniformity facilitates a fair comparison of battery cycling performance, allowing for the assessment of the impact of the different side chains in the DS-RAPs. Initial cycling tests focused on the charge/discharge characteristics alongside accessible capacity through galvanostatic cycling at room temperature across a voltage range of 2.0 to 3.6 V vs Li/Li$^+$ at a low C-rate of 0.1C, which corresponds to a 0.028 mA/cm^2

https://doi.org/10.1021/acs.macromol.4c01894
Macromolecules 2024, 57, 10410−10417

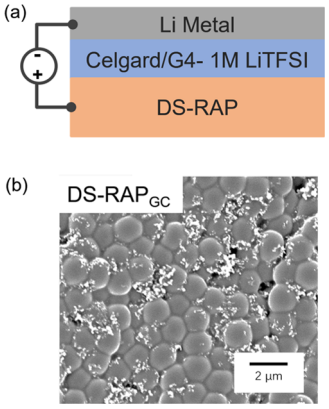

Figure 3. (a) Schematic drawing of coin cell setup consisting of Li metal as an anode, separated by Celgard 2325 porous separator, cathode electrode assembly consisting of DS-RAP, and 1 M LiTFSI in tetraglyme (G4) as electrolyte. (b) SEM image of the cathode electrode composite with 90 wt % DS-RAP$_{GC}$, 5 wt % of poly(vinylidene fluoride), and 5 wt % of carbon black (CB) coated on carbon paper (CP) demonstrating uniform particle assembly.

applied current density (Figure 4). This applied current density was calculated based on the theoretical capacity of DS-RAPs used in this study (64 mAh/g), assuming a two-electron transfer mechanism for the reduction/oxidation of the disulfide redox center (eq S2).

The resulting charge/discharge profiles at 0.1C are shown in Figure 4a. The measured potential profile is consistent with the redox potentials obtained from the CV measurements. This consistency is further validated through the differential capacity (dQ/dV) profiles of the charge/discharge cycles, as shown in Figure S5. In Figure 4b, the 0.1C specific charge capacity (SCC) and specific discharge capacity (SDC), averaged across nine cycles, are presented for each DS-RAP derivative. Note that the DS-RAP$_{EPX}$, which contains residual epoxides, demonstrated the lowest performance with a specific charge capacity (SCC) of 16.6 mAh/g and a specific discharge capacity (SDC) of 14.5 mAh/g (Figure S6) and continuous capacity fade. The lower measured SDC and SCC are attributed to the formation of S−C bonds from the reaction between thiolates and residual epoxides on DS-RAP$_{EPX}$. This reaction irreversibly diminishes disulfide functionalities, thereby reducing the accessible reversible capacity of DS-RAP$_{EPX}$. Overall, increasing the polarity of DS-RAPs enhances capacity accessibility. Among the derivatives, DS-RAP$_{GC}$ exhibited the highest SCC of 63.1 mAh/g and SDC of 53.8 mAh/g at 0.1C. DS-RAP$_{EGA}$ followed, with an SCC of 46.4 mAh/g and an SDC of 43.0 mAh/g. DS-RAP$_{MBA}$ displayed the lowest values, with an SCC of 22.3 mAh/g and an SDC of 18.1 mAh/g.

Efficiency metrics were calculated to further evaluate the performance characteristics of these DS-RAPs at 0.1C (Figure 4c). Here, the Coulombic efficiency (CE) refers to the accessible capacity from the oxidation of thiolates to disulfides during charging relative to the accessible capacity from the reduction of disulfides to thiolates upon discharging. The three DS-RAP derivatives exhibited similar CE within the margin of error, with DS-RAP$_{GC}$ exhibiting a slightly higher average CE of 87.4%. Values less than 100% CE indicate a difference in the accessible state of charge between oxidation and reduction, pointing to potential charge trapping during the reductive discharging of DS-RAPs. The voltage efficiency (VE) of DS-RAP$_{GC}$ was also the highest at 87.8%, attributed to better

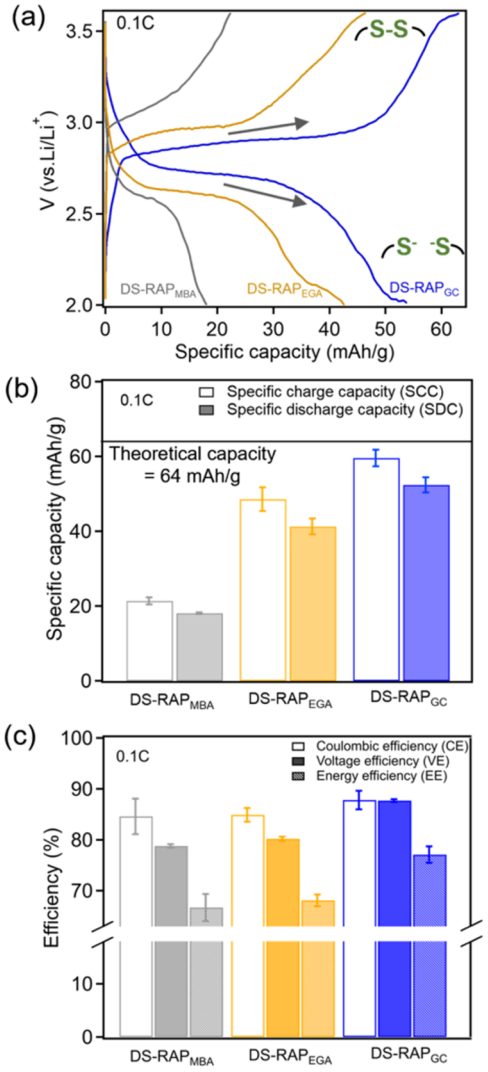

Figure 4. (a) Representative charge/discharge profiles of coin cells cycled at a rate of 0.1C, employing DS-RAPs as the cathode, Li metal as the anode, and a 1 M LiTFSI solution in tetraglyme (G4) as the electrolyte. (b) The corresponding specific charge capacity (SCC) and specific discharge capacity (SDC) of each DS-RAP. (c) Comparison of Coulombic efficiency (CE), voltage efficiency (VE), and energy efficiency (EE) of DS-RAPs.

electrochemical oxidation/reduction kinetics. This was evidenced by the smallest voltage hysteresis among the derivatives (Figure 4a), as seen in the charge/discharge profiles and differential capacity plots (Figure S5). Finally, DS-RAP$_{GC}$ achieved the highest energy efficiency (EE) of 77.1% at 0.1C, driven by its superior VE, marking it as the most efficient in terms of both accessible capacity and efficiency metrics arising from favorable kinetics at low C-rates.

C-Rate Cycling Performance of DS-RAPs. To further evaluate cycling rate capability, lithium cells with DS-RAP cathodes were tested at room temperature from 0.05C to 1C, followed by a return to 0.1C and 0.05C to assess the stability of the accessible capacity during extended sequential C-rate cycling (Figure 5). The representative charge/discharge profiles are shown in Figure S7. As expected, the SCC and SDC of all three DS-RAP derivatives decreased with the increase in C-rate. Upon return to 0.1C and 0.05C, all three DS-RAP derivatives showed that the accessible capacity is

https://doi.org/10.1021/acs.macromol.4c01894
Macromolecules 2024, 57, 10410−10417

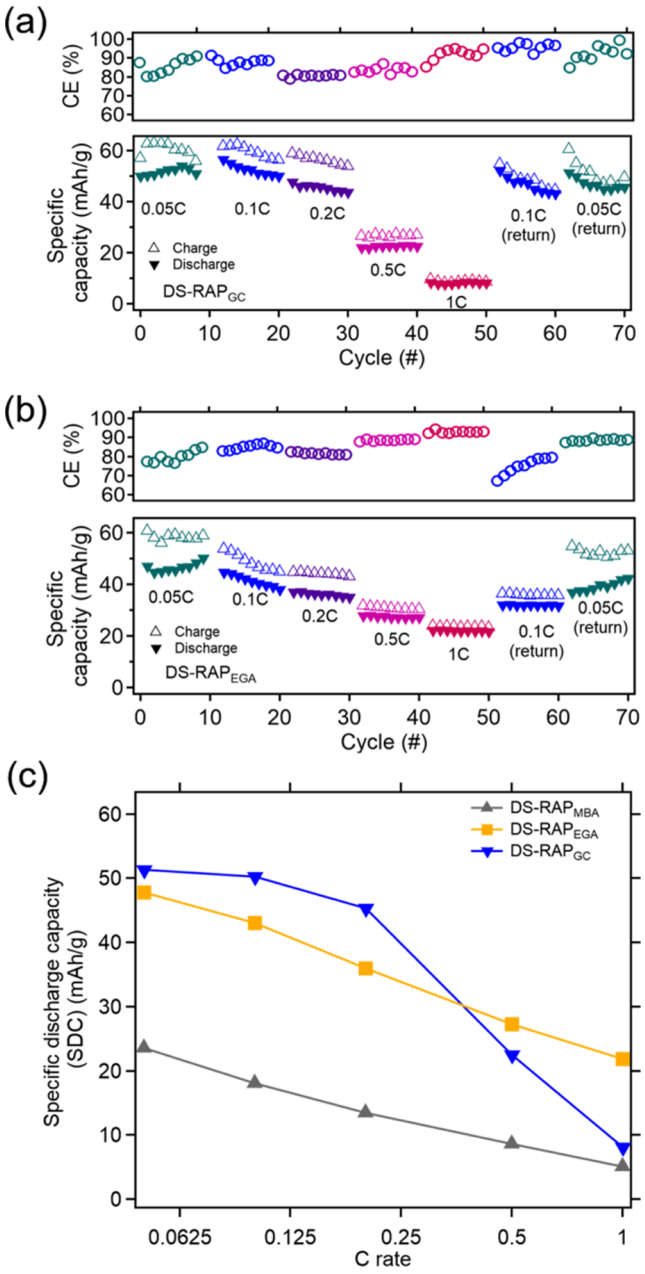

Figure 5. (a) Charge and discharge specific capacities and Coulombic efficiency (CE) at various C-rates for (a) DS-RAP$_{GC}$ and (b) DS-RAP$_{EGA}$. Each cell underwent nine cycles at every C-rate. (c) Modified Peukert plot comparing the trend in specific discharge capacity (SDC) as a function of C-rate for the three DS-RAPs. The reported SDC is the average value of the nine cycles of each C-rate.

recovered, indicating that higher rate cycling does not detrimentally affect their stability. Interestingly, the extent of the decrease in SCC and SDC with C-rate varies between the DS-RAPs. Across C-rates from 0.05C to 0.2C, DS-RAP$_{GC}$ consistently outperformed in SCC and SDC. At 0.05C, it achieved an average SCC of 60.4 ± 2.5 mAh/g and SDC of 51.6 ± 1.3 mAh/g, with a CE of 85.6 ± 3.8%, similar to its performance at 0.1C (Figure 5a). At a higher C-rate (0.5C and 1C), a significant drop in SCC and SDC was observed for DS-RAP$_{GC}$, with SCC decreasing to 8.6 ± 0.4 mAh/g and SDC to 8.0 ± 0.2 mAh/g at 1C. However, at the higher C-rates of 0.5C and 1C, DS-RAP$_{EGA}$ began to outperform DS-RAP$_{GC}$, maintaining an SDC of 27.3 ± 0.3 mAh/g at 0.5C and continued to exhibit higher performance of SDC of 21.8 ± 0.2 mAh/g at 1C. Nonpolar DS-RAP$_{MBA}$ showed the lowest SCC and SDC across the full range of C-rates compared to polar DS-RAP$_{GC}$ and DS-RAP$_{EGA}$ (Figure S8). A modified Peukert plot was employed to illustrate these observations, plotting the average SDC of each DS-RAP variant over the range of C-rates, which highlighted the better performance of DS-RAP$_{GC}$ at lower C-rates and that of DS-RAP$_{EGA}$ at higher C-rates (Figure 5c).

The difference in the C-rate dependent accessible capacity between the DS-RAPs is hypothesized to arise, in part, from the electrolyte swelling influenced by the side chain functional group of the particle, which impacts the ion transport characteristics. Note that dry particle sizes of the DS-RAP derivatives were identical (~1.60 μm in diameter by SEM). Particle sizes in their swelled state were quantified through optical microscope images of particles in a 1 M LiTFSI in G4 electrolyte solution (Figure S9). The diameter of nonpolar DS-RAP$_{MBA}$ particles was measured at 2.10 ± 0.11 μm, a 33% increase from the dry state. By comparison, polar side chain functionalized DS-RAPs exhibited enhanced swelling. DS-RAP$_{GC}$ particles had a swollen diameter of 2.37 ± 0.13 μm, representing a 49% increase in diameter, while DS-RAP$_{EGA}$ particles displayed the most significant swelling, with a diameter of 2.80 ± 0.17 μm, equating to a 76% increase in diameter from the dry state. This augmented swelling capability facilitates improved ion transport within the particles, thereby enhancing electrochemical access. The enhanced mass transport of ions is particularly advantageous at higher C-rates, which could partially account for the larger SDC observed for DS-RAP$_{EGA}$.

To further substantiate this hypothesis, ion diffusivities of the three DS-RAP derivatives were determined using the galvanostatic intermittent titration technique (GITT) (Figure S10).[27−31] GITT involves an alternating sequence of current pulses interspersed with zero current relaxation periods. Following the application of a 10 min current pulse, cell potential rises sharply due to the *iR* drop that occurs in the electrical circuit on account of the current (i) flowing through it and the resistance (R), the total of uncompensated resistance (R_u) and charge transfer resistance (R_{ct}). The resulting diffusion coefficients revealed notable trends; as a baseline, the ion diffusivity for DS-RAP$_{MBA}$ was measured to be 1.18 × 10^{-9} cm^2/s (Table S3). DS-RAP$_{GC}$ exhibited a significantly enhanced ion diffusivity of 3.61 × 10^{-9} cm^2/s, indicating a 305% improvement over DS-RAP$_{MBA}$. DS-RAP$_{EGA}$ showed the highest lithium diffusion coefficient at 4.37 × 10^{-9} cm^2/s, a 370% increase. The significant increase in diffusion coefficients from the electrolyte swollen particles helps explain the heightened capacity accessed from DS-RAP functionalized with EGA and GC side chains.

Extended Cycling and Capacity Recovery in DS-RAPs. A long-term cycling test on the DS-RAPs was performed at 0.1C across 400 cycles to assess capacity retention and cycling stability (Figure 6). Here, the discussion will focus on DS-RAP$_{GC}$ and DS-RAP$_{EGA}$, which had the highest accessible capacity (data for DS-RAP$_{MBA}$ is shown in Figure S11). DS-RAP$_{EGA}$, after 100 cycles, exhibited an SDC of 38.6 mAh/g, preserving 96.7% of its initial capacity, demonstrating notable short-term capacity retention. Over extended cycling (400 cycles), its capacity declined to 21.8 mAh/g, or a retention of 54.6% of the original capacity. By comparison, DS-RAP$_{GC}$

https://doi.org/10.1021/acs.macromol.4c01894
Macromolecules 2024, 57, 10410−10417

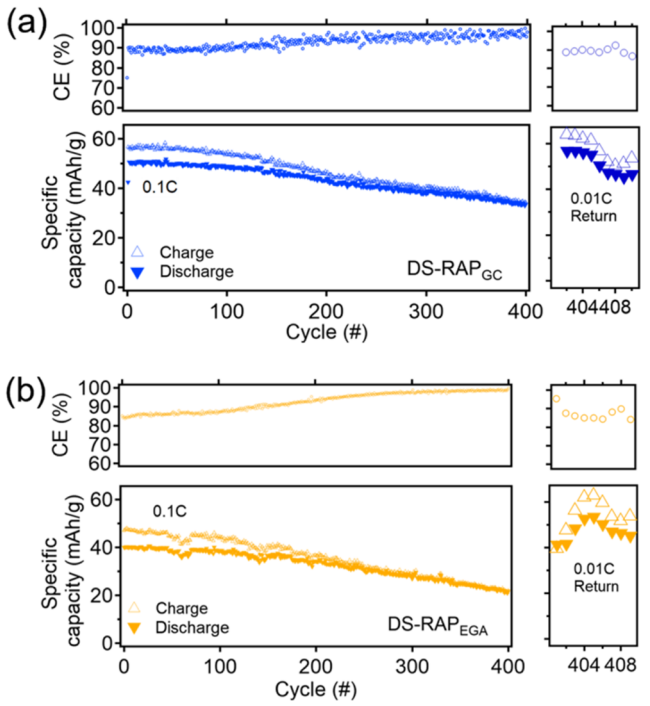

Figure 6. Long-term cycling analysis of Coulombic efficiency (CE) and specific charge/discharge capacity of (a) DS-RAP$_{GC}$ and (b) DS-RAP$_{EGA}$ were conducted at 0.1C over 400 cycles and then cycled at a lower rate of 0.01C for 10 additional cycles.

began with a higher SDC of 50.4 mAh/g, which slightly decreased to 48.8 mAh/g after 100 cycles, resulting in a capacity retention of 96.8%. After 400 cycles, this material maintained a capacity of 33.4 mAh/g, equating to a retention of 66.3% of its initial capacity. Overall, DS-RAP$_{GC}$ exhibited the best capacity retention. Interestingly, the CE increases across the 400 cycles reaching values of 99.7 and 99.6% for DS-RAP$_{EGA}$ and DS-RAP$_{GC}$, respectively.

After 400 cycles at 0.1C, the coin cells were then tested at a significantly lower C-rate of 0.01 to understand the extent of recovery of capacity. For both derivatives, a substantial portion of their SCC and SDC were recovered at 0.01C. Specifically, the recovered SDC for DS-RAP$_{GC}$ was 46.3 mAh/g, with a CE of 89.6%. For DS-RAP$_{EGA}$, the recovered SDC was 47.3 mAh/g, with a CE of 87.3%. For comparison, fresh cells were prepared and tested at 0.01C for 10 cycles where DS-RAP$_{EGA}$ exhibited a capacity of 49.2 mAh/g with a CE of 94.5%, while DS-RAP$_{GC}$ showed a capacity of 54.1 mAh/g with a CE of 96.0% (Figure S12). The difference in the 0.01C data between extended cycling and fresh coin cells suggests that both DS-RAPs undergo a small level of degradation over 400 cycles. However, the substantial recovery of specific capacities post long-term cycling confirms that degradation is not the primary reason for the gradual decrease in the specific capacities of DS-RAP$_{GC}$ and DS-RAP$_{EGA}$ over the 400 cycles, which is likely attributable to charge trapping, as discussed earlier from the analysis of CE at 0.1C. The data suggest that charge trapping occurs during the reductive discharging of DS-RAPs, resulting in a smaller fraction of the overall capacity being accessible after each consecutive charge/discharge step across the 400 cycles, leading to the increasing CE shown in the long term cycling data.

CONCLUSIONS

The synthesis and electrochemical characterization of redox-active disulfide particles (DS-RAPs) with different side chain moieties have been presented. CV measurements indicate that polar side chain moieties improve the electrochemical accessibility of DS-RAPs when tested in electrolytes based on acetonitrile and tetraglyme. The glycidyl carbonate containing DS-RAP$_{GC}$ exhibited the highest CV current response and smallest peak-to-peak separation, indicating comparatively better kinetics relative to the particles with oligoethylene glycol amine (DS-RAP$_{EGA}$) or alkyl functionalized side chains (DS-RAP$_{MBA}$). When testing DS-RAPs as electrodes in a Li-metal cell, DS-RAP$_{GC}$ exhibited the highest SCC of 63.1 mAh/g and SDC of 53.8 mAh/g at 0.1C (theoretical specific capacity = 64 mAh/g), significantly improved over DS-RAP$_{MBA}$ (SCC of 22.3 mAh/g and an SDC of 18.1 mAh/g). Moreover, the calculation of efficiency metrics revealed that DS-RAP$_{GC}$ exhibited the highest voltage efficiency (VE) and energy efficiency (EE) due to its better oxidation/reduction kinetics at 0.1C. Cycling rate tests showed that SCC and SDC decreased as expected but recovered upon return to 0.1C and 0.05C for all three DS-RAP derivatives, indicating stability despite higher rate cycling. Interestingly, cycling measurements at high C-rates revealed that DS-RAP$_{EGA}$ has a higher accessible specific capacity compared to DS-RAP$_{GC}$ and DS-RAP$_{MBA}$. These results suggest that DS-RAP$_{EGA}$ is more resilient to mass transport limitations at higher C-rates likely arising from greater electrolyte swelling and highest ion diffusivity, as determined by GITT measurements. Long-term cycling at 0.1C across 400 cycles showed that DS-RAP$_{GC}$ exhibited the least capacity fade, with charge trapping likely occuring during the reductive discharging of the DS-RAPs, being a key factor contributing to this fade. Overall, this study demonstrates a facile approach to molecular engineering of organic redox-active polymers, enhancing cycling performance through side chain modifications that increase the polarity of DS-RAPs without altering the redox center. These findings providing valuable insights into designing effective organic materials for energy storage applications.

ASSOCIATED CONTENT

Supporting Information

The Supporting Information is available free of charge at https://pubs.acs.org/doi/10.1021/acs.macromol.4c01894.

Experimental section includes synthesis details of all DS-RAP derivatives, FT-IR, UV−vis, SEM, size measurement via optical microscope, galvanostatic cycling, and GITT of DS-RAPs (PDF)

AUTHOR INFORMATION

Corresponding Authors

Stuart J. Rowan − *Pritzker School of Molecular Engineering, University of Chicago, Chicago, Illinois 60637, United States; Joint Center for Energy Storage Research and Chemical Sciences and Engineering Division, Argonne National Laboratory, Argonne, Illinois 60439, United States; Department of Chemistry, University of Chicago, Chicago, Illinois 60637, United States;* orcid.org/0000-0001-8176-0594; Email: stuartrowan@uchicago.edu

Shrayesh N. Patel − *Pritzker School of Molecular Engineering, University of Chicago, Chicago, Illinois 60637, United States; Joint Center for Energy Storage Research and Chemical*

https://doi.org/10.1021/acs.macromol.4c01894
Macromolecules 2024, 57, 10410−10417

Sciences and Engineering Division, Argonne National Laboratory, Argonne, Illinois 60439, United States; orcid.org/0000-0003-3657-827X; Email: shrayesh@uchicago.edu

Authors

Hongyi Zhang − *Pritzker School of Molecular Engineering, University of Chicago, Chicago, Illinois 60637, United States; Joint Center for Energy Storage Research, Argonne National Laboratory, Argonne, Illinois 60439, United States*

Garrett L. Grocke − *Pritzker School of Molecular Engineering, University of Chicago, Chicago, Illinois 60637, United States; Joint Center for Energy Storage Research, Argonne National Laboratory, Argonne, Illinois 60439, United States;* orcid.org/0000-0001-8661-5038

George Rose − *Pritzker School of Molecular Engineering, University of Chicago, Chicago, Illinois 60637, United States*

Complete contact information is available at: https://pubs.acs.org/10.1021/acs.macromol.4c01894

Notes

The authors declare no competing financial interest.

■ ACKNOWLEDGMENTS

The authors gratefully acknowledge financial support from the Joint Center for Energy Storage Research (JCESR), an Energy Innovation Hub funded by the U.S. Department of Energy, Office of Science, Basic Energy Sciences (BES). This work made use of the shared facilities at the University of Chicago Materials Research Science and Engineering Center, supported by the National Science Foundation under award number DMR-2011854. Parts of this work were carried out at the Soft Matter Characterization Facility of the University of Chicago.

■ REFERENCES

(1) Ambrose, H.; Kendall, A. Understanding the Future of Lithium: Part 1, Resource Model. *J. Ind. Ecol.* **2020**, *24* (1), 80−89.
(2) Kim, J.; Kim, Y.; Yoo, J.; Kwon, G.; Ko, Y.; Kang, K. Organic Batteries for a Greener Rechargeable World. *Nat. Rev. Mater.* **2023**, *8* (1), 54−70.
(3) Lu, Y.; Zhang, Q.; Chen, J. Perspectives on the Redox Chemistry of Organic Electrode Materials in Lithium Batteries. *CCS Chem.* **2023**, *5* (7), 1491−1508.
(4) Liang, Y.; Tao, Z.; Chen, J. Organic Electrode Materials for Rechargeable Lithium Batteries. *Adv. Energy Mater.* **2012**, *2* (7), 742−769.
(5) Wang, D. Y.; Guo, W.; Fu, Y. Organosulfides: An Emerging Class of Cathode Materials for Rechargeable Lithium Batteries. *Acc. Chem. Res.* **2019**, *52* (8), 2290−2300.
(6) Guo, W.; Wang, D. Y.; Chen, Q.; Fu, Y. Advances of Organosulfur Materials for Rechargeable Metal Batteries. *Adv. Sci.* **2022**, *9* (4), No. 2103989.
(7) Liu, M.; Visco, S. J.; De Jonghe, L. C. Novel Solid Redox Polymerization Electrodes: Electrochemical Properties. *J. Electrochem. Soc.* **1991**, *138* (7), No. 1896.
(8) Liu, M.; Visco, S. J.; De Jonghe, L. C. Novel Solid Redox Polymerization Electrodes: All-Solid-State, Thin-Film, Rechargeable Lithium Batteries. *J. Electrochem. Soc.* **1991**, *138* (7), No. 1891.
(9) Zhang, S. C.; Zhang, L.; Wang, W. K.; Xue, W. J. A Novel Cathode Material Based on Polyaniline Used for Lithium/Sulfur Secondary Battery. *Synth. Met.* **2010**, *160* (17−18), 2041−2044.
(10) Deng, S.-R.; Kong, L.-B.; Hu, G.-Q.; Wu, T.; Li, D.; Zhou, Y.-H.; Li, Z.-Y. Benzene-Based Polyorganodisulfide Cathode Materials for Secondary Lithium Batteries. *Electrochim. Acta* **2006**, *51* (13), 2589−2593.
(11) Naoi, K.; Kawase, K.; Mori, M.; Komiyama, M. Electrochemistry of Poly(2,2′-dithiodianiline): A New Class of High Energy Conducting Polymer Interconnected with S−S Bonds. *J. Electrochem. Soc.* **1997**, *144* (6), No. L173.
(12) Grocke, G. L.; Zhang, H.; Kopfinger, S. S.; Patel, S. N.; Rowan, S. J. Synthesis and Characterization of Redox-Responsive Disulfide Cross-Linked Polymer Particles for Energy Storage Applications. *ACS Macro Lett.* **2021**, *10* (12), 1637−1642.
(13) Karami, H.; Mousavi, M. F.; Shamsipur, M. A New Design for Dry Polyaniline Rechargeable Batteries. *J. Power Sources* **2003**, *117* (1−2), 255−259.
(14) Hauffman, G.; Maguin, Q.; Bourgeois, J.-P.; Vlad, A.; Gohy, J.-F. Micellar Cathodes from Self-Assembled Nitroxide-Containing Block Copolymers in Battery Electrolytes. *Macromol. Rapid Commun.* **2014**, *35* (2), 228−233.
(15) Oh, S. H.; Lee, C. W.; Chun, D. H.; Jeon, J. D.; Shim, J.; Shin, K. H.; Yang, J. H. A Metal-Free and All-Organic Redox Flow Battery with Polythiophene as the Electroactive Species. *J. Mater. Chem. A* **2014**, *2* (47), 19994−19998.
(16) Wu, S.; Zhao, Y.; Li, D.; Xia, Y.; Si, S. An Asymmetric Zn//Ag Doped Polyaniline Microparticle Suspension Flow Battery with High Discharge Capacity. *J. Power Sources* **2015**, *275*, 305−311.
(17) Montoto, E. C.; Nagarjuna, G.; Hui, J.; Burgess, M.; Sekerak, N. M.; Hernández-Burgos, K.; Wei, T.-S.; Kneer, M.; Grolman, J.; Cheng, K. J.; et al. Redox Active Colloids as Discrete Energy Storage Carriers. *J. Am. Chem. Soc.* **2016**, *138* (40), 13230−13237.
(18) Zhuo, S.; Tang, M.; Wu, Y.; Chen, Y.; Zhu, S.; Wang, Q.; Xia, C.; Wang, C. Size Control of Zwitterionic Polymer Micro/Nanospheres and Its Dependence on Sodium Storage. *Nanoscale Horiz.* **2019**, *4* (5), 1092−1098.
(19) Li, X.; Li, Y.; Sarang, K.; Lutkenhaus, J.; Verduzco, R. Side-Chain Engineering for High-Performance Conjugated Polymer Batteries. *Adv. Funct. Mater.* **2021**, *31* (14), No. 2009263.
(20) Lee, S.; Kwon, G.; Ku, K.; Yoon, K.; Jung, S. K.; Lim, H. D.; Kang, K. Recent Progress in Organic Electrodes for Li and Na Rechargeable Batteries. *Adv. Mater.* **2018**, *30* (42), No. 1704682.
(21) Schon, T. B.; McAllister, B. T.; Li, P. F.; Seferos, D. S. The Rise of Organic Electrode Materials for Energy Storage. *Chem. Soc. Rev.* **2016**, *45* (22), 6345−6404.
(22) Paulsen, B. D.; Tybrandt, K.; Stavrinidou, E.; Rivnay, J. Organic Mixed Ionic−Electronic Conductors. *Nat. Mater.* **2020**, *19* (1), 13−26.
(23) Chung, J.; Khot, A.; Savoie, B. M.; Boudouris, B. W. 100th Anniversary of Macromolecular Science Viewpoint: Recent Advances and Opportunities for Mixed Ion and Charge Conducting Polymers. *ACS Macro Lett.* **2020**, *9* (5), 646−655.
(24) Gallastegui, A.; Minudri, D.; Casado, N.; Goujon, N.; Ruipérez, F.; Patil, N.; Detrembleur, C.; Marcilla, R.; Mecerreyes, D. Proton Trap Effect on Catechol-Pyridine Redox Polymer Nanoparticles as Organic Electrodes for Lithium Batteries. *Sustainable Energy Fuels* **2020**, *4* (8), 3934−3942.
(25) Bartels, J.; Wang, J.-H. H.; Chen, Q.; Runt, J.; Colby, R. H. Segmental Dynamics of Ethylene Oxide-Containing Polymers with Diverse Backbone Chemistries. *Macromolecules* **2016**, *49* (5), 1903−1910.
(26) You, D.; Hu, W.; Song, L.; Wei, W.; Xiong, H. High-Energy Metallic Lithium Batteries Enabled by Polymer-in-Salt Electrolytes of Cyclic Carbonate Substituted Polyethers. *ACS Appl. Polym. Mater.* **2022**, *4* (11), 8584−8593.
(27) Shaju, K. M.; Rao, G. V. S.; Chowdari, B. V. R. EIS and GITT Studies on Oxide Cathodes, O2-Li(2/3)+x(Co0.15Mn0.85)O2 (x = 0 and 1/3). *Electrochim. Acta* **2003**, *48* (18), 2691−2703.
(28) Shaju, K. M.; Rao, G. V. S.; Chowdari, B. V. R. Influence of Li-Ion Kinetics in the Cathodic Performance of Layered Li(Ni[Sub 1/3]Co[Sub 1/3]Mn[Sub 1/3])O[Sub 2. *J. Electrochem. Soc.* **2004**, *151* (9), No. A1324.
(29) Shaju, K.; Rao, G. S.; Chowdari, B. V. Li-Ion Kinetics and Polarization Effect on the Electrochemical Performance of Li(Ni1/2Mn1/2)O2. *Electrochim. Acta* **2004**, *49* (9−10), 1565−1576.

(30) Zhang, L.; Chen, Y.; Jiang, Z.; Chen, J.; Wei, C.; Wu, W.; Li, S.; Xu, Q. Cation-Anion Redox Active Organic Complex for High Performance Aqueous Zinc Ion Battery. *Energy Environ. Mater.* **2024**, 7 (1), No. e12507.
(31) Lubis, A. L.; Baskoro, F.; Lin, T.-H.; Wong, H. Q.; Liou, G.-S.; Yen, H.-J. Redox-Active High-Performance Polyimides as Versatile Electrode Materials for Organic Lithium- and Sodium-Ion Batteries. *ACS Appl. Mater. Interfaces* **2024**, *16* (37), 48722−48735.

https://doi.org/10.1021/acs.macromol.4c01894
Macromolecules 2024, 57, 10410−10417